Supporting Information

Structural design of biomass-derived hard carbon anode materials for superior sodium storage via increasing crystalline cellulose and closing the open pores

Xiaoying Li[1], Sijing Zhang[1], Jingjing Tang[1*], Juan Yang[1], Kang Wen[2], Jiong Wang[2], Peng Wang[3], Xiangyang Zhou[1], Yaguang Zhang[1]

1 School of Metallurgy and Environment, Central South University, Changsha 410083, Hunan, China

2 Chenyu-Fuji New Energy Technology Company Limited, Changsha 410083, Hunan, China

3 Dali Chenyu Energy Storage New Material Company Limited, DaLi 671000, Yunan, China

*Corresponding author

Email address: tangjj@csu.edu.cn.

Experimental

Material synthesis

Almond (Badam) shells from Xinjiang in northwest China were crushed into fine powder by a small high-speed grinder. The almond shell powder was firstly stirred in 2.25 M HF solution at room temperature for 6 h to remove inorganic impurities. After that, it was washed with deionized water to neutral and dried in the oven at 80 ℃ overnight. To enhance the cellulose crystallinity and regulate the amorphous component content within the precursors, the purified powder was stirred in 6 M and 10 M HCl solution, respectively, at room temperature for 6 h. Then, the powder was washed with deionized water and dried in the oven at 80 ℃ overnight. The obtained precursors, along with that solely treated with HF solution, were subjected to carbonization at 600 ℃ for 2 h in a tubular furnace under argon flow, with a heating rate of 5 ℃ min^{-1}. After cooling to room temperature, the pre-carbonized samples were further carbonized at 1300 ℃ for 3 hours under argon flow with the same heating rate. The resultant hard carbon materials were denoted as A-2.25, A-2.25-6, and A-2.25-10, respectively. A sample treated with 2.25 M HF and 6 M HCl underwent a two-step pre-carbonization to investigate the influence of heating rate and residence temperature. This sample experienced a gradual temperature increase to 400 ℃ at a rate of 1 ℃ min^{-1} for 1 h, followed by a ramp to 600 ℃ at 5 ℃ min^{-1} for 1 hour before cooling to room temperature. Subsequently, the sample underwent carbonization under identical high-temperature conditions as the other samples and was designated as A-2.25-6-T.

Material characterization

Fourier transform infrared spectroscopy (FTIR) was performed using an infrared spectrometer (Thermo Scientific Nicolet iS50). The microcrystalline structure of all samples was

characterized by X-ray diffraction (XRD, PANalytical Empyrean 2 with Cu Kα radiation (λ = 0.154 nm)) and Raman spectra using a Confocal micro raman spectrometer (Renishaw inVia Reflex). The nitrogen adsorption-desorption isothermal curves were tested on a Micromeritics ASAP 2460 analyzer to obtain the Branauer-Emmett-Teller (BET) specific surface area and pore size distribution. The morphology and structure of resulting samples were analyzed by field emission scanning electron microscopy (SEM, ZEISS Sigma 300) and a high-resolution transmission electron microscope (HRTEM, Talos F200X). The closed pores of all samples were characterized by Small-angle X-ray scattering (SAXS, Xenocs Xeuss 2.0, sample test distance is 2480 mm). Thermo gravimetry-Differential scanning calorimetry (TG-DSC, Netzsch STA 449 F3) was used to study the pyrolysis process of precursor. Gases generated during pyrolysis were characterized by Thermal gravimetric analysis combined with mass spectrometry (TG-MS, TA Instrument, SDT 650+ Discovery MS) to analyze the structural evolution of hard carbon material. X-ray photoelectron spectroscopy (XPS, Thermo Scientific K-Alpha) was recorded to represent the chemical state of the sample surface. After discharging or charging to the specified voltage, coin cells were disassembled in a glove box and the electrodes were washed with 1,2-dimethoxyethane (DME) and dried. Then, the electrodes were sealed in a container for ex-situ XRD and Raman measurement.

Electrochemical measurements

The electrochemical performance was measured using CR2016 coin-type half cells assembled in an argon-filled glovebox (Mikrouna, H_2O, O_2 < 0.1 ppm). The slurry of electrodes was prepared by uniformly mixing 90 wt.% almond shell-derived hard carbon powder, 5 wt.% sodium alginate (SA), 5 wt.% carbon black in an appropriate amount of deionized water. Before

assembling the cells, the pasted electrode obtained by coating the mixed slurry on copper foil was dried at 80 °C for 12 h under vacuum. The mass loading of active material is around 1 mg cm^{-2}. Glass fiber (Whatman GF/A) and sodium foil were used as separators and the counter electrode. The electrolyte was a solution of 1 M NaPF$_6$ in DME. The galvanostatic charged/discharged and galvanostatic intermittent titration technique (GITT) tests were operated on LAND-CT2001A battery systems (LAND Electronic Co., Wuhan, China) with a voltage range of 0.01-2.0 V (vs. Na$^+$/Na). In the full cells, the hard carbon anode was matched with the NVP cathode. The NVP electrode was prepared by mixing 80 wt.% NVP, 10 wt.% PVDF, 10 wt.% carbon black in an appropriate amount of NMP solution. The pasted electrode obtained by coating the mixed slurry on aluminum foil was dried at 80 °C for 24 h under vacuum. To ensure the overall performance of the full cell, the mass ratio of NVP and hard carbon was kept at 2.5:1. The charge/discharge cut-off voltage was set to 2-4 V, and the specific capacity was calculated based on the mass of NVP only. For the GITT test, the pulse current was set at 20 mA g^{-1} for 10 min and an interval of 2 h. An electrochemical workstation (PARSTAT MC, AMETEK) was used to record cyclic voltammetry (CV) at different scan rates of 0.2-3 mV s^{-1} between 0.01-2 V (vs. Na$^+$/Na) and electrochemical impedance spectroscopy (EIS) between 0.01-10^5 Hz.
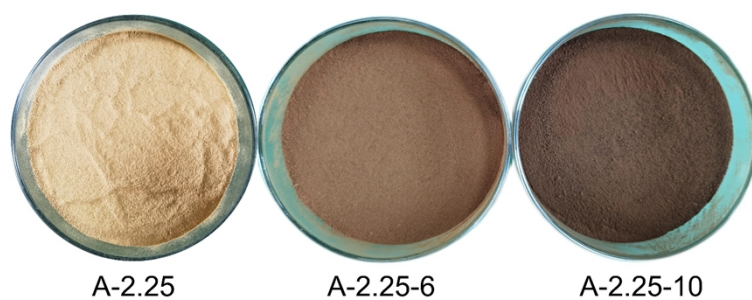
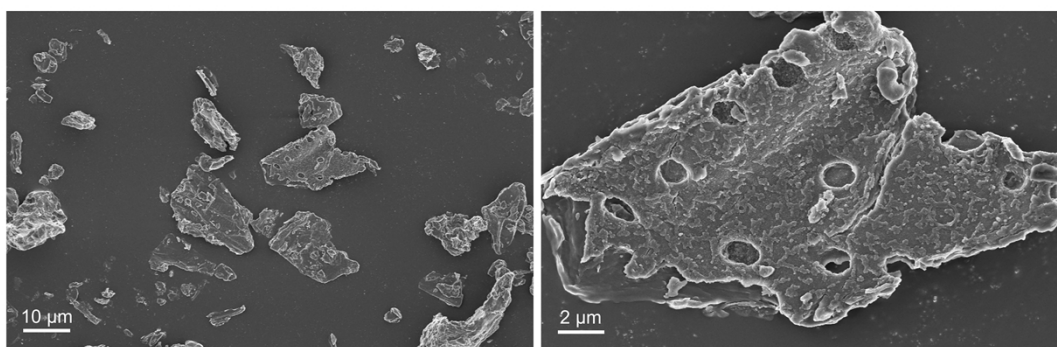Fig. S1. Optical photographs of acid-treated precursors

Fig. S2. SEM images of precursor without acid treatment

Table S1 Component analysis(wt.%) of almond shell

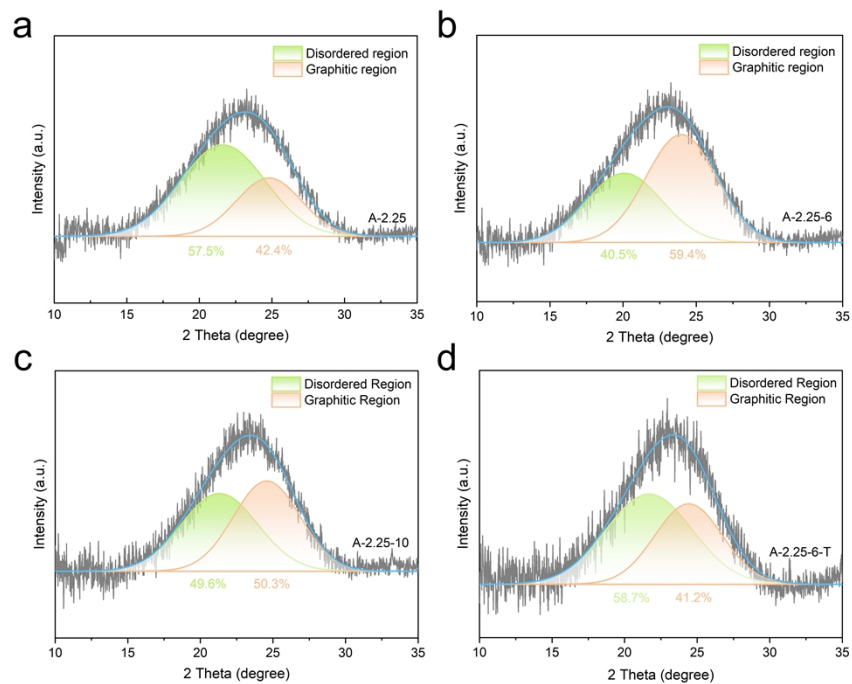| Samples	cellulose	hemicellulose	lignin	water	ashes	volatile
almond shell	27.3	20.8	31.9	2.91	1.78	71.62
A-2.25	29.6	20.1	33.4	3.42	0.4	78.1
A-2.25-6	33.9	15.1	37.9	4.63	0.33	73.3
A-2.25-10	45.4	/	45.3	7.3	0.22	73.0

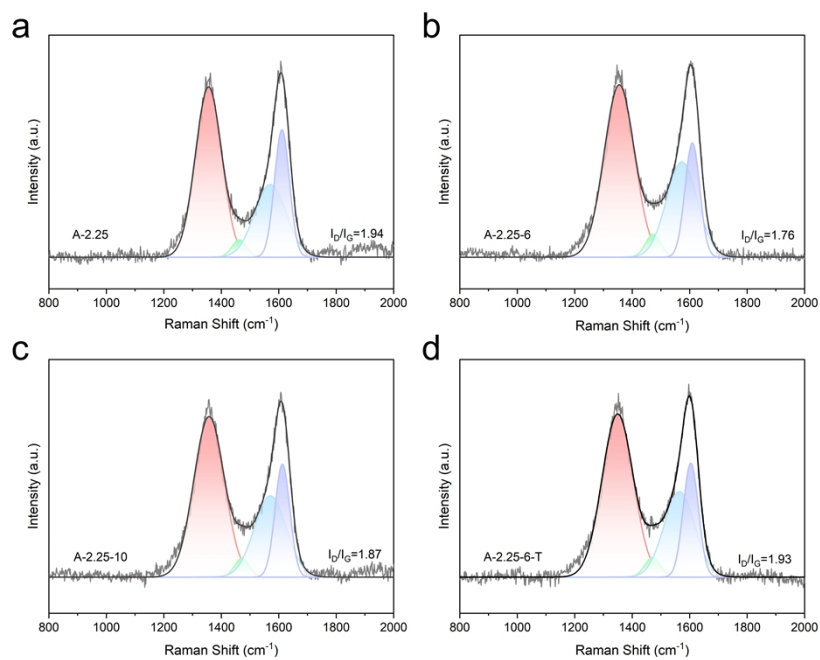Fig. S3. 002 fitting peak of (a) A-2.25, (b) A-2.25-6, (c) A-2.25-10, (d) A-2.25-6-T

Fig. S4. Deconvoluted Raman spectra of (a) A-2.25, (b) A-2.25-6, (c) A-2.25-10, (d) A-2.25-6-T
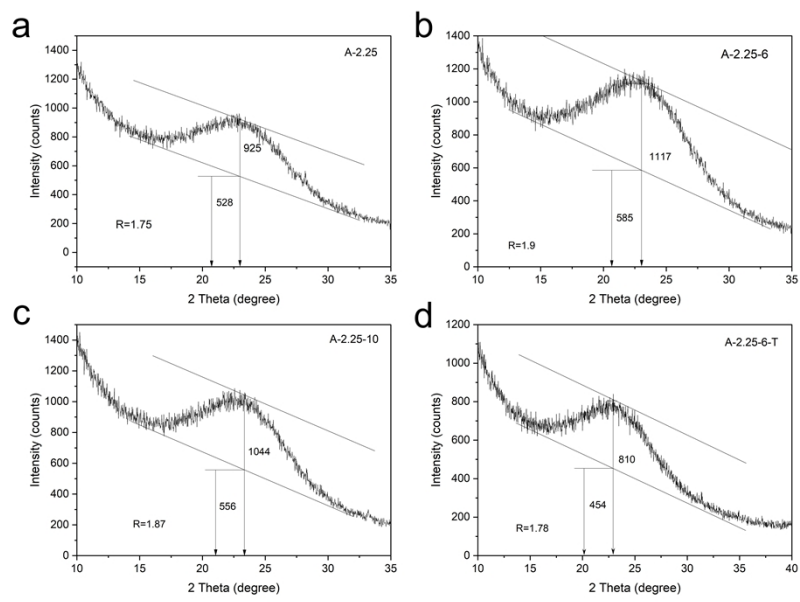
Fig. S5. Schematic diagram of the calculation of R-value from peak 002 for (a) A-2.25, (b) A-2.25-6, (c) A-2.25-10, (d) A-2.25-6-T
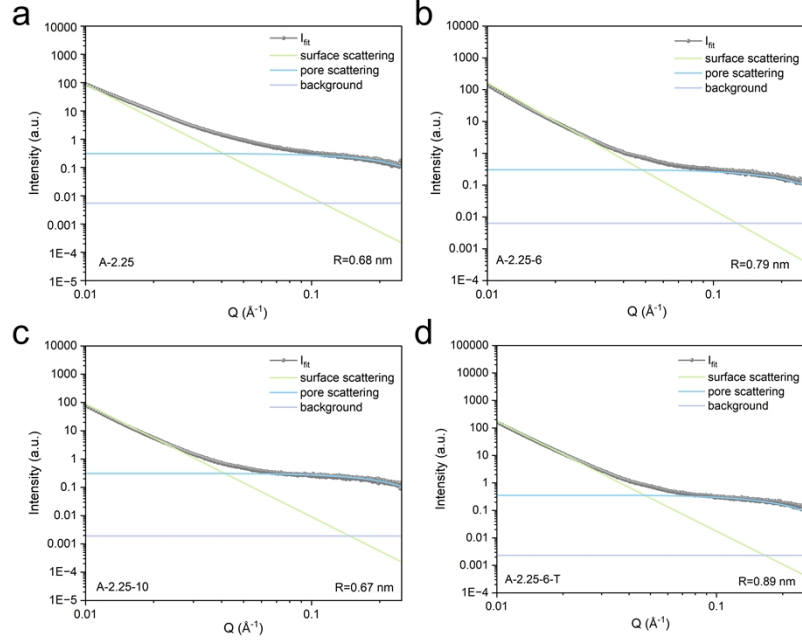
Fig. S6. Fitted SXAS patterns of (a) A-2.25, (b) A-2.25-6, (c) A-2.25-10, (d) A-2.25-6-T

The SAXS patterns are fitted based on the following model[1]:

$$I(q) = \frac{A}{q^4} + \frac{B'a_1^4}{(1 + a_1^2 q^2)^2} + D$$

$I(q)$: scattered intensity as a function of q.

q: scattering vector.

A: proportional to the total surface areas of the large pores.

B': proportional to the total surface areas of the small pores.

a_1: the characteristic length over which electron density variations occur.

D: constant background term.

The radius of the pores can be obtained from the formula: $R = a_1\sqrt{10}$.
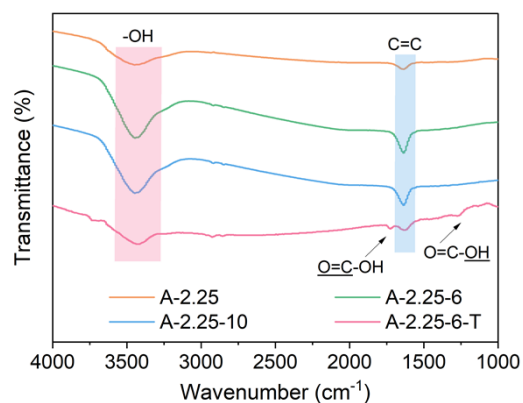
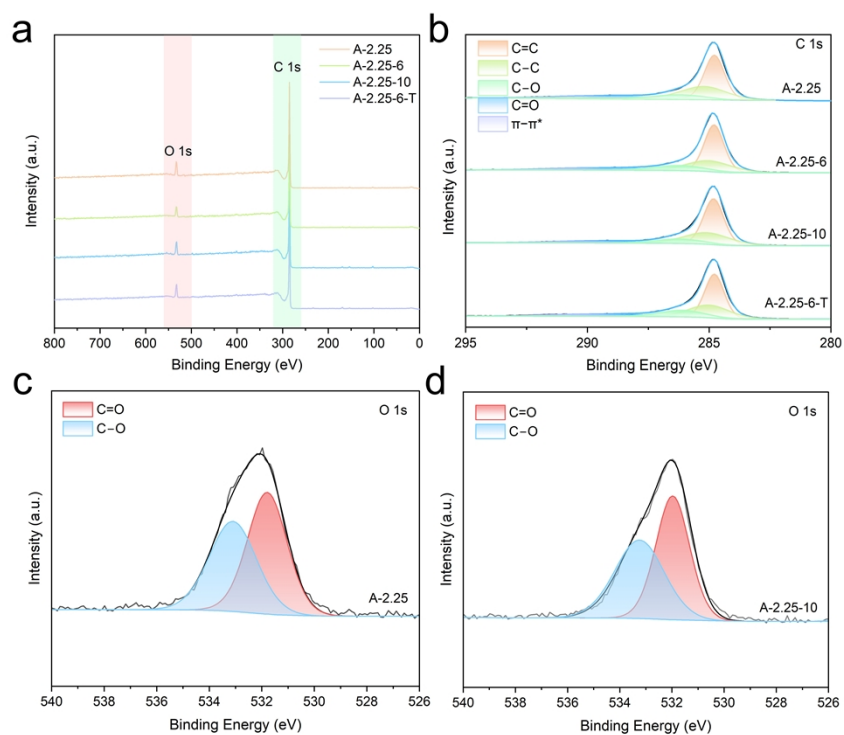Fig. S7 FT-IR spectra of A-2.25, A-2.25-6, A-2.25-10, A-2.25-6-T

Fig. S8. XPS spectra (a) and C 1s high-resolution spectra (b) of A-2.25, A-2.25-6, A-2.25-10, A-2.25-6-T, O 1s high-resolution spectra of (c) A-2.25 and (d) A-2.25-10

Table S2 The element contents of C and O in A-2.25, A-2.25-6, A-2.25-10, and A-2.25-6-T samples

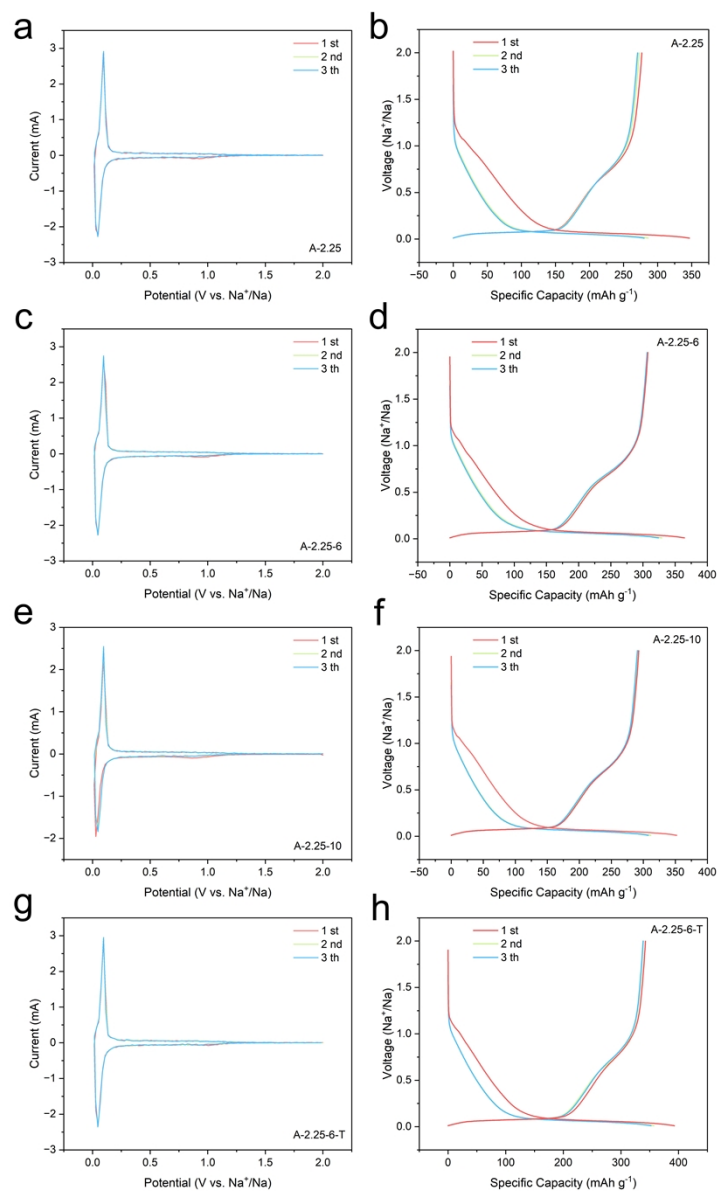| Samples	Atomic %	
	C	O
A-2.25	92.97	7.03
A-2.25-6	93.29	6.71
A-2.25-10	93.07	6.93
A-2.25-6-T	92.98	7.02

Fig. S9. CV curves at a scan rate of 0.2 mV s^{-1} (a, c, e, g) and galvanostatic discharge/charge profiles at 0.03 A g^{-1} (b, d, f, h) of A-2.25, A-2.25-6, A-2.25-10, A-2.25-6-T

Table S3 Electrochemical performance of almond shell derived-hard carbon

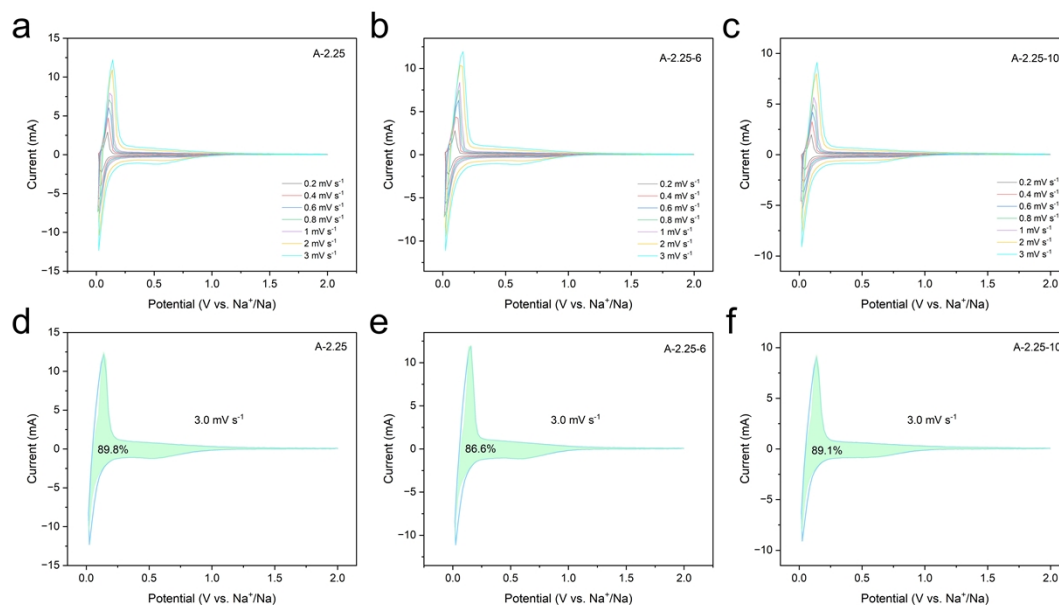| Samples	Charge capacity (mAh g^{-1})	ICE (%)	Retention ratio after 500 cycles(%)
A-2.25	276.8	79.83	81.41
A-2.25-6	319.5	82.57	87.43
A-2.25-10	292.8	83.18	87.24
A-2.25-6-T	342.4	87.19	87.03

Fig. S10. (a-c) CV curves at various scan rates from 0.2 to 3.0 mV s^{-1} and (d-f) CV curves with a calculated capacitive contribution at 3 mV s^{-1} of A-2.25, A-2.25-6, and A-2.25-10
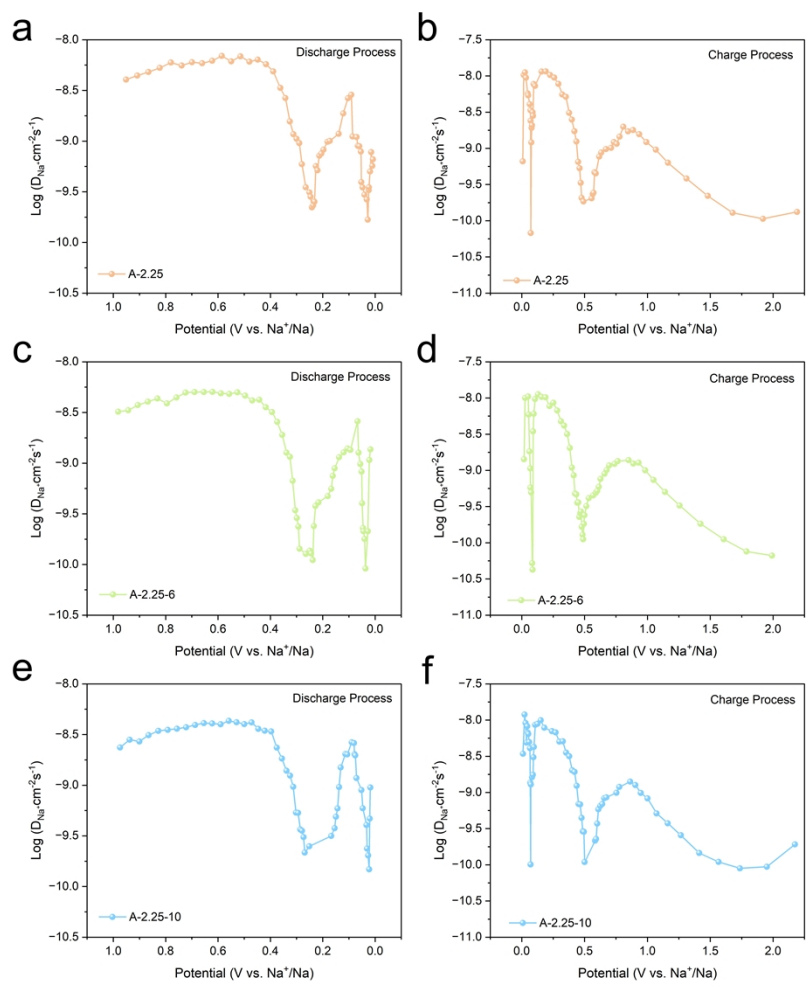
Fig. S11. Na$^+$ diffusion coefficients calculated from the GITT potential profiles of (a-b) A-2.25, (c-d) A-2.25-6, and (e-f) A-2.25-10
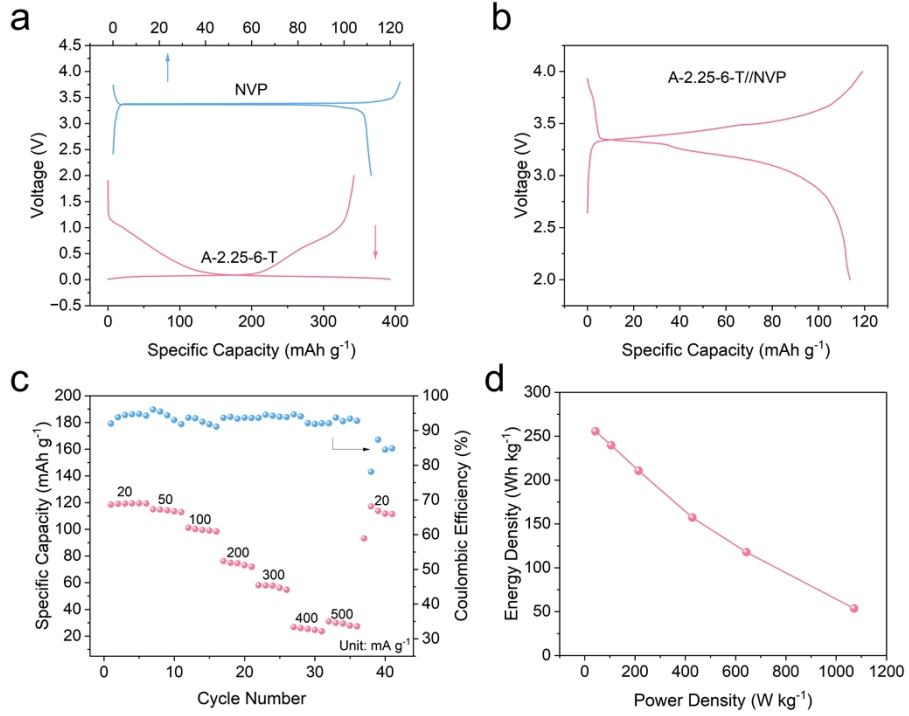
Fig. S12. (a) Galvanostatic discharge/charge profiles of NVP and A-2.25-6-T in half cells, electrochemical performance characterization of the NVP//A-2.25-6-T full cell: (b) initial galvanostatic discharge/charge profiles at 20 mA g^{-1}, (c) rate performance, (d) energy density and power density at various current densities.

The power density and energy density of the full cells were calculated by following equations[2]:

$P = (\Delta V \times I) / m$

$\Delta V = (V_{max} + V_{min}) / 2$

$E = (P \times t) / 3600$

where I is the discharge current, t is the discharge time, m is the total loading mass of active materials, V_{max} and V_{min} are the voltage at the beginning and end of discharge, respectively.

Table S4 Comparison of electrochemical performance of hard carbon anode in this work with reported related materials for sodium-ion batteries

Samples	Raw materials	Reversible capacity (mAh g^{-1})	ICE (%)	Rate capacity (mAh g^{-1})	Ref.
Hard carbon	almond shell	342.4, 0.01-2 V, 30 mA g^{-1}	87.19	189.6 at 5A g^{-1}	This work
Bamboo-derived hard carbon	bamboo powder	348.5, 0-2.5 V, 30 mA g^{-1}	84.1	206.5 at 2 A g^{-1}	[3]
Agar-derived porous carbon	agar and phytic acid	439, 0.01-3 V, 50 mA g^{-1}	30.98	140 at 5A g^{-1}	[4]
Chitosan-derived hard carbon	chitosan	317.4, 0.01-3 V, 500 mA g^{-1}	70.59	238.9 at 5A g^{-1}	[5]
Bio-spore-derived hard carbon	spores of Calvatia Gigantea	438.5, 0-3 V, 25 mA g^{-1}	90.23	254.8 at 5A g^{-1}	[6]
Balloon-like porous hard carbon	puffball	205.05, 0.01-3 V, 100 mA g^{-1}	57.6	102.12 at 10 A g^{-1}	[7]
N, O, S tri-doping turbostratic carbon	4, 6-diamino-2(1h)-pyrimidinethione	321.5, 0.01-3 V, 100 mA g^{-1}	55.53	175.5 at 5A g^{-1}	[8]
N-doped carbon nanosheets	carboxymethyl cellulose and g-C$_3$N$_4$	304.7, 0-2.5 V, 50 mA g^{-1}	79.52	197.6 at 5A g^{-1}	[9]
Porous carbon sphere@void@carbon	anhydrous glucose	216.7, 0.01-3 V, 100 mA g^{-1}	85.3	140.3 at 10 A g^{-1}	[10]

Reference

[1] D.-A. Stevens, J.-R. Dahn, An In Situ Small-Angle X-Ray Scattering Study of Sodium Insertion into a Nanoporous Carbon Anode Material within an Operating Electrochemical Cell, J. Electrochem. Soc. 147 (2000) 4428, https://doi.org/10.1149/1.1394081c.

[2] D. Sun, L. Zhao, P.-L. Sun, K. Zhao, Y.-K. Sun, Q. Zhang, Z.-C. Li, Z. M, F.-Z. Zheng, Y. Yang, C.-B. Lu, C. Peng, C.-M. Xu, Z.-H. Xiao, X.-L. Ma, Rationally Regulating Closed Pore Structures by Pitch Coating to Boost Sodium Storage Performance ofHard Carbon in Low-voltage Platforms, Adv. Funct. Mater. (2024) https://doi.org/10.1002/adfm.202403642.

[3] T.-Y. Xu, X. Qiu, X. Zhang, Y.-Y. Xia, Regulation of surface oxygen functional groups and pore structure of bamboo-derived hard carbon for enhanced sodium storage performance, Chem. Eng. J. 452 (2023) 139514, https://doi.org/10.1016/j.cej.2022.139514.

[4] T. Wang, L.-L. Liu, Y.-W. Wei, Y.-H. Gao, S. Wang, D.-Q. Jia, W. Zhang, J.-Q. Sha, Agar-Derived Slope-Dominated Carbon Anode with Puparium Like Nano-Morphology for Cost-Effective SIBs, Small (2023) 2309809, https://doi.org/10.1002/smll.202309809.

[5] H.-L. Sun, Q.-Y. Zhang, F. Yuan, D. Zhang, Z.-J. Li, Q.-J. Wang, H. Wang, B. Wang, Unraveling the effect of carbon morphology evolution in hard carbons on sodium storage performance, Inorg. Chem. Front. 10 (22) (2023) 6547-6556, https://doi.org/10.1039/D3QI01497E.

[6] T.-J. Tang, W.-L. Zhu, P.-P. Lan, X.-X. Lan, H.-R. Xie, P.-K. Shen, Z.-Q. Tian, Macro-micro structure engineering of bio-spore-derived hard carbon as an efficient anode in sodium ion batteries, Chem. Eng. J. 475 (2023) 146212, https://doi.org/10.1016/j.cej.2023.146212.

[7] L.-H. Yu, L.-L. Zhang, X.-D. He, X. Tao, G.-Z. Zhao, H.-L. Xie, R.-L. Zhu, G. Zhu, Study of stable sodium ion storage in porous carbon derived from puffball biomass, Ind. Crop. Prod. 208 (2024) 117805, https://doi.org/10.1016/j.indcrop.2023.117805.

[8] D.-C. Qin, L. Wang, X.-X. Zeng, J. Shen, F. Huang, G.-Y. Xu, M.-F. Zhu, Z.-H. Dai, Tailored edge-heteroatom tri-doping strategy of turbostratic carbon anodes for high-rate performance lithium and sodium-ion batteries, Energy Storage Mater. 54 (2023) 498-507, https://doi.org/10.1016/j.ensm.2022.10.049.

[9] Y.-H. Zhao, Z. Hu, C.-L. Fan, P. Gao, R.-S. Zhang, Z.-X. Liu, J.-S. Liu, J.-L. Liu, Novel Structural Design and Adsorption/Insertion Coordinating Quasi-Metallic Na Storage Mechanism toward High-performance Hard Carbon Anode Derived from Carboxymethyl Cellulose, Small 19 (41) (2023), https://doi.org/10.1002/smll.202303296.

[10] D.-J. Cheng, Z..-H. Li, M.-L. Zhang, Z.-H. Duan, J. Wang, C.-Y. Wang, Engineering Ultrathin Carbon Layer on Porous Hard Carbon Boosts Sodium Storage with High Initial Coulombic Efficiency, ACS Nano 17 (19) (2023) 19063-19075, https://doi.org/10.1021/acsnano.3c04984.